Diagn Interv Radiol 2026; DOI: 10.4274/dir.2025.253652

INTERVENTIONAL RADIOLOGY

ORIGINAL ARTICLE

Association between magnetic resonance imaging-based prostatic tissue morphology and changes in International Prostate Symptom Score and maximum urinary flow rate after prostatic artery embolization

Chen Wang[1]
Kun Liang[1]
Jiasheng Qin[1]
Xin Shu[1]
Lihua Yuan[1]
Jianfei Dong[2]

[1]Department of Interventional Radiology, Nanjing Drum Tower Hospital, Affiliated Hospital of Medical School, Nanjing University, Nanjing, China

[2]Department of Otorhinolaryngology Head and Neck Surgery, Nanjing Drum Tower Hospital, Affiliated Hospital of Medical School, Nanjing University, Nanjing, China

PURPOSE

To evaluate whether baseline multiparametric magnetic resonance imaging (mpMRI)-defined prostate morphological phenotypes are associated with changes in the International Prostate Symptom Score (ΔIPSS) and maximum urinary flow rate (ΔQmax) following prostatic artery embolization (PAE) in patients with benign prostatic hyperplasia (BPH).

METHODS

This retrospective single-center study included patients who underwent technically successful PAE with preprocedural mpMRI performed within 8 weeks of intervention. Prostate morphology was classified as glandular-dominant, stromal-dominant, or mixed phenotype based on the predominant nodule signal characteristics on T2-weighted imaging (T2WI), with supplemental assessment using diffusion-weighted and contrast-enhanced sequences when available. Symptomatic and functional outcomes—ΔIPSS and ΔQmax—were assessed at 3, 6, 12, and 24 months post-procedure. Associations between morphology and outcomes were evaluated using multivariable regression and subgroup analysis.

RESULTS

A total of 152 patients (mean age, 70.0 ± 9.9 years) who underwent technically successful PAE were included in the study, all of whom had preprocedural MRI performed within 8 weeks prior to the intervention. All MRI-defined morphological phenotypes demonstrated improvements in the Qmax and IPSS after PAE. The glandular-dominant phenotype exhibited the most pronounced and earliest response, with peak improvements at 6 months (ΔQmax: 10.45 mL/s; ΔIPSS: 14.11 points) and sustained benefits through 24 months (ΔQmax: 8.78 mL/s; ΔIPSS: 13.04 points). Stromal-dominant and mixed phenotypes showed smaller, delayed improvements, typically peaking at 12 months. Morphology-related phenotype differences remained statistically significant at 24 months in unadjusted comparisons, particularly between glandular and stromal phenotypes, although ΔIPSS differences were attenuated in multivariable models (24-month β: 0.104, $P = 0.547$). Glandular morphology was consistently associated with a greater ΔQmax across all timepoints (e.g., 24-month β: 0.450, $P < 0.001$) and significantly interacted with baseline symptom severity (IPSS ≥ 20) to predict enhanced 24-month ΔIPSS (interaction β: 0.349, $P = 0.045$). Subgroup analyses stratified by prostate volume (< 80 vs. ≥ 80 mL) corroborated these findings, with glandular morphology consistently outperforming that of stromal and mixed phenotypes.

CONCLUSION

Baseline MRI-defined prostate morphology, assessed primarily on T2WIs, was significantly associated with clinical outcomes after PAE; glandular-dominant morphology was linked to larger and more sustained improvements in both the Qmax and IPSS. Therefore, MRI-based phenotypes offer a practical imaging biomarker for patient stratification, warranting prospective validation.

CLINICAL SIGNIFICANCE

The MRI-based classification of prostate morphology may improve patient selection and predict clinical outcomes following PAE in BPH management.

KEYWORDS

Benign prostatic hyperplasia, lower urinary tract symptoms, prostatic artery embolization, magnetic resonance imaging, prostate morphology

Handling editor: İlkay İdilman

Corresponding author: Lihua Yuan

E-mail: lihua.yuan@njglyy.com

Corresponding author: Jianfei Dong

E-mail: alaterbloomer@sina.com

Received 22 September 2025; revision requested 01 November 2025; last revision requested 19 December 2025; accepted 29 December 2025.

Epub: 26.01.2026

Publication date: 01.07.2026

DOI: 10.4274/dir.2025.253652

You may cite this article as: Wang C, Liang K, Qin J, Shu X, Yuan L, Dong J. Association between magnetic resonance imaging-based prostatic tissue morphology and changes in International Prostate Symptom Score and maximum urinary flow rate after prostatic artery embolization. *Diagn Interv Radiol*. 2026;32(4):463-472.

Benign prostatic hyperplasia (BPH) is a prevalent condition among aging men, characterized by non-malignant proliferation of epithelial and stromal components within the prostatic transition zone. This histologic expansion contributes to lower urinary tract symptoms (LUTS), including increased urinary frequency, urgency, and nocturia and a reduced urinary stream. Pharmacologic therapies—primarily α-adrenergic antagonists and 5α-reductase inhibitors—remain the first-line treatment; however, their efficacy is often limited and is associated with adverse effects such as hypotension, ejaculatory dysfunction, and poor long-term adherence. For patients with moderate-to-severe LUTS or an unsatisfactory response to medication, transurethral resection of the prostate (TURP) has long served as the gold-standard surgical intervention, providing rapid and durable symptom relief in most cases.[1,2] More recently, prostatic artery embolization (PAE) has emerged as a minimally invasive alternative that achieves prostate debulking through selective arterial occlusion, leading to ischemia and subsequent tissue necrosis. Unlike TURP, PAE does not require general anesthesia and is particularly suitable for elderly individuals, patients with substantial comorbidities, or those seeking nonsurgical options. Clinical studies have demonstrated that PAE effectively alleviates LUTS and improves quality of life; however, therapeutic responses remain heterogeneous, and reliable imaging biomarkers for outcome prediction are lacking.[3-6] Multiparametric magnetic resonance imaging (mpMRI), combining T2-weighted imaging (T2WI), diffusion-weighted imaging (DWI), and dynamic contrast-enhanced (DCE) sequences, has become the standard for comprehensive prostate evaluation. It provides a unified framework for lesion characterization across institutions. The Prostate Imaging Reporting and Data System PI-RADS v2.1 (American College of Radiology, Reston, VA, USA). standardizes the acquisition and interpretation of prostate MRI to detect clinically significant prostate cancer, particularly in the peripheral zone, where the majority of clinically significant prostate cancer occurs. Although PI-RADS assesses the transition zone, it is primarily designed to assess malignant lesions, and its utility in distinguishing benign changes, such as BPH, in the transition zone is limited. The transition zone, where stromal and glandular nodules exhibit heterogeneous morphology and signal patterns, is not sufficiently addressed by PI-RADS. Recent studies on BPH have emphasized the use of quantitative MRI-derived metrics, such as transition zone volume and transition zone index, which correlate with surgical enucleation volume and bladder outlet obstruction. These findings underscore the need for a dedicated classification system to assess benign changes in the transition zone.[7,8] Histopathologic investigations emphasize that BPH encompasses a spectrum of nodular hyperplasia with varying proportions of glandular and stromal elements, resulting in substantial tissue and imaging heterogeneity. Glandular-dominant nodules primarily consist of epithelial structures and glandular lumina, whereas stromal-dominant nodules contain abundant smooth muscle and fibrous tissue.[9] Clinically, patients with adenomatous-dominant BPH (AdBPH) have been shown to achieve greater prostate volume reduction and more pronounced symptomatic improvement following PAE, suggesting that imaging-based morphological subtyping may hold prognostic value.[10]

Building on these histologic insights, mpMRI has been explored as a non-invasive tool for preprocedural morphological characterization. In particular, T2-weighted and DWI features have been correlated with underlying tissue composition.[11] Glandular-dominant nodules typically exhibit high T2 signal intensity and correspond to improved post-PAE outcomes, whereas stromal-dominant patterns—characterized by a low T2 signal and dense fibromuscular stroma—are associated with less favorable responses.[12]

Despite these encouraging findings, a standardized and clinically applicable MRI-based classification system for prostate morphology has not been widely validated. In this study, we propose a T2-weighted MRI classification framework that categorizes transition zone nodules into three phenotypes: glandular dominant, stromal dominant, and mixed. We aimed to evaluate whether MRI-defined prostate morphological phenotypes are associated with changes in the International Prostate Symptom Score (IPSS) and maximum urinary flow rate (Qmax) following PAE. To explore potential effect modification, prespecified subgroup analyses stratified by the baseline prostate volume (< 80 vs. ≥ 80 mL) were also conducted.[13]

Main points

- Magnetic resonance imaging-based prostate morphology classification into glandular-dominant, stromal-dominant, and mixed phenotypes provides a practical imaging surrogate for underlying histologic composition in benign prostatic hyperplasia.
- Glandular-dominant prostates demonstrated the most pronounced and consistent improvements in both the International Prostate Symptom Score (IPSS) and maximum urinary flow rate (Qmax) after prostatic artery embolization, with the maximal response observed at 6 months and sustained benefits identified through long-term follow-up.
- Stromal-dominant and mixed phenotypes exhibited delayed or attenuated benefits, typically reaching their peak effect at around 12 months.
- Subgroup analysis revealed a morphology- and volume-dependent gradient of efficacy, with interphenotype differences in functional outcomes (ΔQmax) emerging earlier in larger prostates (≥ 80 mL).
- Magnetic resonance imaging-defined glandular-dominant morphology, particularly in patients with a high baseline IPSS, was independently associated with sustained symptomatic and functional benefits at 24 months.

Methods

Study design and patient selection

This study initially included 220 patients diagnosed with BPH-related LUTS. Of these, 68 were excluded because they did not meet the requirements of the inclusion criteria, with 152 patients ultimately included (as outlined in the flowchart, Figure 1, Table 1).

This retrospective single-center study was approved by the Ethics Committee of Nanjing Drum Tower Hospital, The Affiliated Hospital of Nanjing University Medical School (reference number: 2024-124-02, date: April 24, 2024), and the requirement for informed consent was waived due to the retrospective nature of the study. We screened consecutive patients who underwent PAE for symptomatic BPH between May 2020 and March 2022. A total of 152 patients (mean age, 70.0 ± 9.9 years) who underwent technically successful PAE were included in the study, all of whom had preprocedural MRI performed within 8 weeks prior to intervention.

Patients were eligible for inclusion if they had an IPSS of ≥ 15 at baseline, experienced persistent moderate-to-severe LUTS refractory to standard pharmacologic treatment, underwent multiparametric pelvic MRI within 8 weeks prior to embolization, and completed follow-up assessments at 3, 6, 12, and 24 months post-procedure. Exclusion criteria included prior prostate surgery, neurogenic bladder, known or suspected prostate malignancy, technical failure of embolization, or incomplete imaging or clinical data.

Baseline variables, including age, body mass index (BMI), total prostate volume (TPV), and MRI-defined morphology (glandular, stromal, mixed), were extracted from institutional electronic medical records. The prolate ellipsoid formula (TPV = 0.52 × transverse × anteroposterior × craniocaudal dimensions) was used to calculate TPV, measured on axial and sagittal T2WIs, which is the standard method recommended in contemporary prostate MRI protocols.

Prostate biopsy was not performed routinely and was only pursued when malignancy was clinically suspected (e.g., elevated or rising prostate-specific antigen levels, abnormal digital rectal examination, or MRI findings suggestive of malignancy). A small number of patients were diagnosed with prostate cancer during follow-up, either due to the absence of preprocedural suspicion warranting biopsy or as a result of false-negative preprocedural assessments. These cases were marked as exclusions in the flowchart (Figure 1). Although PI-RADS v2.1 scoring is included in standard institutional MRI reporting, it was not utilized in this study. Our focus was on evaluating benign transition zone morphology, a feature not adequately addressed by PI-RADS, which is primarily designed to detect malignant lesions in the peripheral zone. Although PI-RADS includes the transition zone in its evaluation, its primary application is to assess clinically significant prostate cancer, providing limited guidance for the assessment of BPH or other benign morphological changes in the transition zone. Therefore, we employed a morphology-based classification system specifically developed for assessing benign features in the transition zone—an aspect not covered by PI-RADS.

Magnetic resonance imaging acquisition and morphological subtyping

Magnetic resonance imaging acquisition

All MRI examinations were performed using either a 1.5-T or 3.0-T scanner (Ingenia CX or UMR platform) equipped with an 8–16-channel phased-array pelvic coil. The standard protocol included multiplanar T2-weighted turbo spin-echo sequences, which served as the primary basis for morphological classification. DWI was performed on all patients as part of the routine clinical protocol during the study period. However, DCE sequences were available only in a limited subset of patients (< 15%) according to the clinical routine at the time of scanning. When present, these sequences were used qualitatively as supportive references to improve tissue characterization or to exclude foci with suspected cancer. When available, the DCE sequences often showed patterns suggestive of early enhancement in gland-rich nodules and more prolonged enhancement in stromal-dominant nodules, consistent with the T2-weighted impressions of the respective tissue composition. However, no quantitative perfusion parameters were analyzed, and classification of nodule morphology was based solely on axial T2WI to maximize consistency across the cohort.[14,15] Acquisition parameters, including field strength, coil type, repetition and echo times, slice thickness, and pixel size, are summarized in Table 2.

Patient preparation procedures were standardized according to institutional protocols. Patients were instructed to fast for at least 6 hours prior to the MRI and PAE procedures. Additionally, for optimal prostate visualization during MRI, patients were asked to maintain a comfortably full bladder.

Morphological subtyping

A phenotypic classification system was developed based on visual assessment of the dominant imaging characteristics of transition zone nodules, categorizing BPH into glandular-dominant, stromal-dominant, and mixed phenotypes. In the glandular-dominant phenotype, glandular nodules were larger and more prominent, predominantly composed of glandular tissue, and showed high signal intensity on T2WI, distinguishing them clearly from the surrounding stromal tissue. The mixed phenotype featured multiple glandular nodules, even when these nodules were not dominant in size. These nodules appeared alongside stromal elements, with alternating high and low signal intensities on T2WI, reflecting the heterogeneous nature of the transition zone. The stromal-dominant phenotype was characterized by minimal or absent glandular nodules, with the lesions predominantly composed of stromal tissue exhibiting low signal intensity, typical of be-

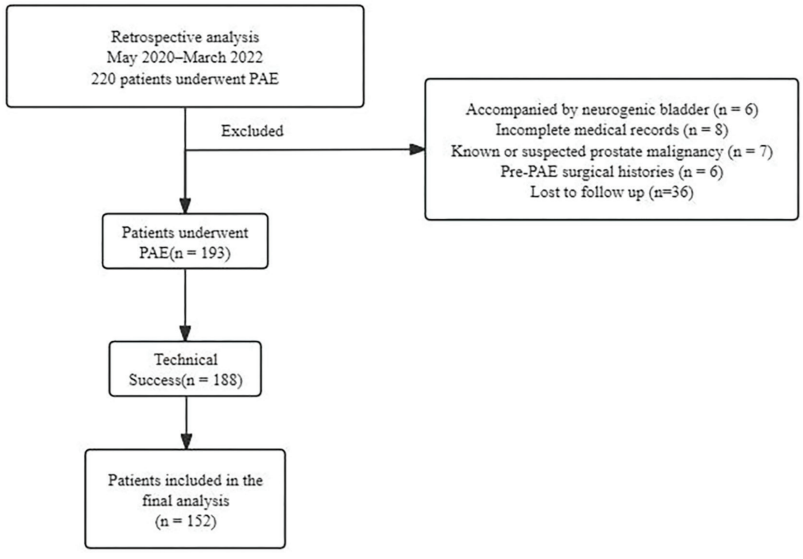

Figure 1. Flowchart illustrating the retrospective analysis design of this study.

PAE, prostatic artery embolization.

Table 1. Baseline characteristics by magnetic resonance imaging-defined prostate morphology

Variable	Glandular (n = 53)	Mixed (n = 61)	Stromal (n = 38)	*P*
Age (years)	70.83 ± 8.77	68.54 ± 10.32	66.63 ± 10.89	0.136
BMI (kg/m^2)	28.48 ± 2.79	27.06 ± 3.15	27.99 ± 2.28	0.027
TPV (mL)	96.53 ± 32.70	98.67 ± 32.46	91.52 ± 23.11	0.523
Baseline IPSS	24.98 ± 4.86	24.95 ± 6.10	22.66 ± 6.52	0.110
Baseline Qmax (mL/s)	6.57 ± 2.42	6.39 ± 1.99	6.76 ± 1.71	0.689

IPSS, International Prostate Symptom Score; Qmax, maximum urinary flow rate; TPV, total prostate volume; BMI, body mass index.

nign fibromuscular tissue. These lesions displayed a lamellar or fibrous texture, with no features suggestive of malignancy, such as irregular margins or a diffuse low signal, which are typical of tumor infiltration (Figure 2).[16]

Interobserver agreement

All examinations were independently evaluated by two radiologists, each with more than 5 years of experience in prostate MRI, who were blinded to the clinical data. Morphologic phenotype (glandular dominant, stromal dominant, or mixed) and TPV (T2-weighted planimetry) were determined for each case. Interobserver agreement for phenotype classification was assessed using Cohen's kappa with 95% confidence intervals (CIs), whereas TPV reproducibility was evaluated using intraclass correlation coefficients (ICCs) from a two-way random-effects, absolute-agreement, single-measure model with 95% CIs. Discrepancies between readers were resolved by consensus, and the agreed results were used for subsequent analyses.[17]

Embolization procedure and technical parameters

PAE was performed in all patients under local anesthesia using a transfemoral approach. Procedures were conducted by two experienced interventional radiologists using a cone-beam computed tomography (CT)-equipped C-arm system (Allura Xper FD20/XperCT, Philips). Selective catheterization of the internal iliac artery was achieved with a 4-Fr Simmons or Cobra catheter. When visualization of the prostatic artery was inadequate, tube angulation was adjusted accordingly. Super-selective catheterization of the prostatic artery was achieved using a 2.4–2.7-Fr microcatheter (e.g., Maestro, Merit Medical) over a 0.014-inch steerable microwire (e.g., Fathom, Boston Scientific). In all cases, intra-arterial nitroglycerin was administered to induce vasodilation, followed by cone-beam CT acquisition to delineate the prostatic arterial supply and exclude extra-prostatic collaterals before embolization. Bilaterally, embolization was performed using the PErFecTED technique. Larger microspheres (300–500 µm) were first injected proximally, followed by distal advancement of the microcatheter beyond potential collateral branches for administration of smaller microspheres (100–300 µm). Embolization was performed using calibrated tris-acryl gelatin microspheres (100–300 and 300–500 µm; Embosphere®, Merit Medical, South Jordan, UT, USA). Embolization was monitored under fluoroscopy and digital subtraction angiography, with the endpoint defined as slow antegrade flow or near-stasis in the prostatic artery without reflux, and decreased perfusion of the prostate on post-embolization angiography.[3,4]

Follow-up and endpoints

Clinical assessments—including the IPSS and Qmax—were obtained at baseline and at 3, 6, 12, and 24 months following PAE. All follow-up evaluations were conducted by board-certified interventional radiologists who were blinded to the MRI-based prostate morphology classification. Longitudinal follow-up at each timepoint was used to assess changes from baseline, expressed as ΔIPSS and ΔQmax. These outcome measures were analyzed according to the baseline MRI-defined prostate morphology, categorized as glandular-dominant, stromal-dominant, and mixed phenotypes. Post-PAE complications and their management were systematically documented using information based on patient interviews, reports from referring physician reports, and a review of medical records.

Subgroup analysis

To evaluate whether TPV influenced treatment outcomes, patients were stratified into two prespecified subgroups (< 80 vs. ≥ 80 mL), consistent with previous PAE studies that applied this threshold for both clinical and procedural considerations.[18-20] Baseline TPV was dichotomized at 80 mL for subgroup analyses, in accordance with the prior PAE-related literature and clinical convention distinguishing moderate-sized from large prostates. Within each subgroup, longitudinal changes in the IPSS and Qmax at 3, 6, 12, and 24 months were compared among the MRI-defined morphological phenotypes (glandular-dominant, stromal-dominant, and mixed types).

Complications

All procedure-related complications were documented prospectively and categorized according to the Cardiovascular and Interventional Radiological Society of Europe (CIRSE) Standards of Practice for Reporting Complications (2018 update). Complications were defined as any deviation from the normal postoperative course and graded as minor (CIRSE grades 1–2) or major (grades 3–6) based on the need for therapy, hospitalization, or permanent sequelae. According to this classification, dysuria, mild hematuria, transient urinary retention, and self-limited pelvic pain were considered minor, whereas any event requiring prolonged hospitalization, repeat embolization, or surgical management were considered major.

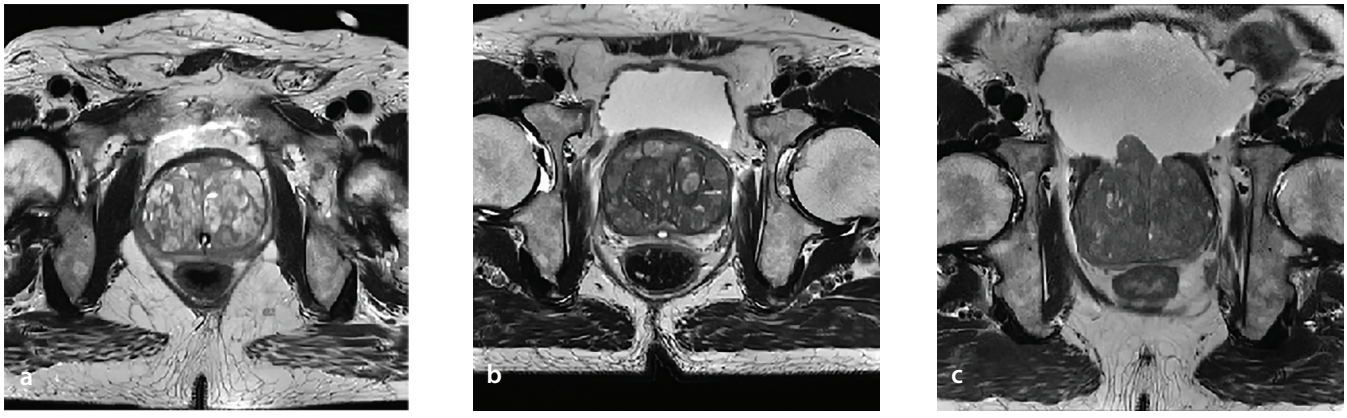

Figure 2. Representative T2-weighted magnetic resonance imaging patterns of transition zone phenotypes in benign prostatic hyperplasia. **(a)** Glandular-dominant phenotype: the transition zone is predominantly composed of glandular nodules, which present as high-signal structures on T2-weighted imaging (T2WI), exhibiting acinous or microcystic morphology. These nodules are easily distinguishable from the surrounding stromal tissue due to their high signal intensity. **(b)** Mixed phenotype: the transition zone shows a combination of glandular and stromal nodules. The glandular nodules are present but not dominant in size, exhibiting alternating high and low signal intensities on T2WI. This phenotype reflects the heterogeneous composition of the transition zone, with both glandular and stromal components clearly visible. **(c)** Stromal-dominant phenotype: the transition zone is primarily composed of stromal nodules, with fewer glandular nodules. The stromal tissue appears as low-signal structures on T2WI, exhibiting a lamellar or fibromuscular texture, typical of benign stromal hyperplasia.

Statistical analysis

All statistical analyses were performed using SPSS (version 31.0; IBM Corp., Armonk, NY, USA) in accordance with the STrengthening the Reporting of OBservational Studies in Epidemiology reporting guidelines.[21] Continuous variables were summarized as mean ± standard deviation and categorical variables as frequencies and percentages. Continuous outcomes (ΔIPSS, ΔQmax) were compared using one-way Analysis of Variance or independent samples t-tests when normality was satisfied. Separate multivariable linear regression models were constructed at each follow-up interval to evaluate associations between baseline variables and clinical outcomes. The ΔIPSS or ΔQmax values served as the dependent variable, whereas prespecified covariates—including age, BMI, baseline TPV, and baseline symptom scores (IPSS for ΔIPSS models; Qmax for ΔQmax models)—were entered as independent variables. To explore potential effect modification, interaction terms between the baseline IPSS and prostate morphology phenotypes were included. Patients were stratified into two categories (IPSS < 20 and IPSS ≥ 20) based on the standard IPSS severity classification, consistent with previous studies that defined IPSS ≥ 20 as indicative of severe symptoms.[22] All statistical tests were two sided, and a P value < 0.05 was considered statistically significant.

Results

Patient characteristics

A total of 152 patients met the inclusion criteria (mean age 70.0 ± 9.9 years). Baseline TPV was comparable among the glandular-dominant, stromal-dominant, and mixed phenotypes. The cohort included 53 patients with glandular-dominant, 38 with stromal-dominant, and 61 with mixed-type morphology, representing 34.9%, 25.0%, and 40.1% of the study population, respectively. The baseline demographic and clinical characteristics summarized by MRI-defined morphology are shown in Table 1. Groups were comparable in age, TPV, baseline IPSS, and baseline Qmax (all $P > 0.05$); BMI differed modestly across phenotypes (overall $P = 0.027$). Across MRI-defined morphological phenotypes, both functional (ΔQmax) and symptomatic (ΔIPSS) outcomes improved significantly after PAE, although the magnitude and timing of improvement differed by phenotype. The glandular-dominant phenotype exhibited the most pronounced and earliest responses, reaching peak improvements at 6 months (ΔQmax: 10.45 mL/s; ΔIPSS: 14.11 points). Minor declines were observed thereafter at 12 and 24 months (ΔQmax: 9.76 and 8.78 mL/s; ΔIPSS: 13.43 and 13.04 points, respectively), yet treatment effects remained substantially above baseline throughout the 24-month follow-up. By contrast, mixed- and stromal-dominant phenotypes demonstrated slower and less marked improvements, with maximal changes occurring at around 12 months for both ΔIPSS and ΔQmax, followed by modest reductions at 24 months. At all follow-up intervals, the glandular-dominant phenotype consistently showed the greatest mean gains in both ΔQmax and ΔIPSS, followed by the mixed and stromal phenotypes. This morphology-dependent gradient in treatment response persisted over time, although the magnitude of intergroup difference slightly attenuated at later timepoints (Table 3).

Multivariable linear regression

Relative to the stromal-dominant reference phenotype, the glandular-dominant phenotype showed greater improvement at 6 months—the timepoint of maximal separation—for both ΔIPSS (β: 0.510, $P < 0.001$) and ΔQmax (β: 0.567, $P < 0.001$). For ΔIPSS, this advantage was also evident at 3 and 12 months but was no longer significant at 24 months. No significant differences in ΔIPSS were observed between the mixed- and stromal-dominant phenotypes at any timepoint. For ΔQmax, the superiority of the glandular-dominant phenotype persisted across all follow-up intervals. Comparisons between mixed and stromal phenotypes revealed higher ΔQmax in the mixed group at 3 and 24 months, with borderline significance at 6 and 12 months. The full model coefficients and corresponding 95% CIs for each timepoint are presented in Table 4. An interaction

Table 2. Magnetic resonance imaging acquisition parameters for prostate imaging sequences

Sequence	TR/TE	FA	ST	Res	Coil	Field	Availability
Axial T2	~4,000/100	120	3–4	0.8–1.2	PA (8–16 ch)	1.5/3.0	All pts
DWI*	Vendor-spec.	—	4–5	1.5–2.0	same	1.5/3.0	All pts
DCE–MRI**	Short TR/TE	10–15	2–4	1.0–1.5	same	1.5/3.0	Subset

*DWI parameters (including TR/TE, b-values, and fat-suppression technique) were vendor-dependent across scanners and were not used for phenotypic classification. **DCE–MRI was acquired using three-dimensional spoiled gradient-echo sequences. Temporal enhancement parameters were not analyzed and did not contribute to phenotypic classification.
T2, T2-weighted imaging; DWI, diffusion-weighted imaging; DCE, dynamic contrast-enhanced MRI; MRI, magnetic resonance imaging; TR, repetition time; TE, echo time; FA, flip angle; ST, slice thickness; Res, in-plane resolution; PA, pelvic array; ch, channels; pts, patients.

Table 3. Interphenotype comparison of ΔIPSS and ΔQmax in all patients

Outcome	Glandular	Mixed	Stromal	*P	**P	***P	****P
ΔQmax 3 m	6.64 ± 2.85	5.45 ± 2.69	4.71 ± 1.72	0.002	0.187	<0.001	0.006
ΔQmax 6 m	10.45 ± 2.32	8.32 ± 2.38	7.36 ± 1.89	< 0.001	< 0.001	<0.001	0.030
ΔQmax 12 m	9.76 ± 2.30	8.59 ± 2.22	7.73 ± 1.83	< 0.001	0.007	<0.001	0.035
ΔQmax 24 m	8.78 ± 2.45	7.46 ± 2.54	6.33 ± 1.97	< 0.001	0.006	<0.001	0.021
ΔIPSS 3 m	7.62 ± 2.96	6.62 ± 2.44	6.11 ± 2.74	0.024	0.051	0.015	0.330
ΔIPSS 6 m	14.11 ± 4.51	10.00 ± 2.86	9.42 ± 2.61	<0.001	<0.001	<0.001	0.314
ΔIPSS 12 m	13.43 ± 3.43	12.36 ± 3.90	11.08 ± 3.77	0.013	0.124	0.003	0.111
ΔIPSS 24 m	13.04 ± 4.28	10.92 ± 3.57	9.16 ± 3.12	<0.001	0.005	<0.001	0.014

*P, overall three-phenotype comparison; **P, glandular vs. mixed; ***P, glandular vs. stromal; ****P, mixed vs. stromal. IPSS, International Prostate Symptom Score; ΔQmax, maximum urinary flow rate; ΔIPSS, change in International Prostate Symptom Score.

between baseline IPSS ≥ 20 and glandular-dominant morphology was identified for ΔIPSS at 24 months (β: 0.349, $P = 0.045$), indicating more pronounced long-term symptomatic improvement among patients with a higher baseline symptom burden and glandular-dominant features.

Subgroup analysis

Subgroup analyses stratified by baseline TPV (< 80 vs. ≥ 80 mL) revealed clear volume-dependent differences in treatment response. In the < 80-mL subgroup, interphenotype variation in ΔQmax was not significant at 3 months but became significant at later timepoints and persisted thereafter. Glandular-dominant prostates showed consistently greater functional improvement than stromal-dominant prostates across all follow-up intervals and also exceeded mixed phenotypes at 6 and 24 months. Mixed and stromal phenotypes did not differ significantly. For ΔIPSS, interphenotype differences at 6 and 24 months were significant, with glandular-dominant morphology associated with greater symptomatic improvement than stromal morphology at all timepoints and with mixed morphology at 6 and 24 months (Table 5). In the ≥ 80 mL subgroup, interphenotype differences in ΔQmax were already significant at 3 months and remained so through 24 months. A clear hierarchical gradient (glandular > mixed > stromal) was observed, with mixed phenotypes separating earlier from stromal-dominant phenotypes in a ΔQmax-a pattern not seen in the smaller-volume subgroup. For ΔIPSS, significant interphenotype variation was again noted at 6 and 24 months, with glandular-dominant morphology showing the greatest improvement, whereas mixed and stromal-dominant phenotypes remained largely comparable (Table 6).

Interobserver agreement

Interobserver agreement was assessed across all 152 patients for both TPV measurements and MRI-based phenotype classification. The ICC for TPV was 0.934, indicating excellent agreement. The Cohen's kappa coefficient for MRI-defined prostate type was 0.836, reflecting very good inter-rater reliability.

Complications

A total of 61 patients (40.1%) experienced minor complications. These included dysuria (n = 19, 12.5%), hematuria (n = 22, 14.5%), urinary tract infections (n = 7, 4.6%), transient urinary retention (n = 14, 9.2%), and pelvic pain (n = 54, 35.5%). Hematospermia occurred in eight patients (5.3%). No major complications were reported in this phenotype.

Table 4. Multivariable regression results

Timepoint	Variable	β coefficient	*P* value
ΔIPSS 3 m	Glandular	0.193	0.048
	Mixed	0.033	0.738
ΔIPSS 6 m	Glandular	0.510	< 0.001
	Mixed	0.024	0.781
ΔIPSS 12 m	Glandular	0.255	0.011
	Mixed	0.120	0.233
ΔIPSS 24 m	Glandular	0.104	0.547
	Mixed	0.269	0.602
	IPSS ≥ 20 × glandular	0.349	0.045
ΔQmax 3 m	Glandular	0.335	< 0.001
	Mixed	0.208	0.038
ΔQmax 6 m	Glandular	0.567	< 0.001
	Mixed	0.179	0.051
ΔQmax 12 m	Glandular	0.415	< 0.001
	Mixed	0.189	0.055
ΔQmax 24 m	Glandular	0.450	< 0.001
	Mixed	0.216	0.027

IPSS, International Prostate Symptom Score; ΔQmax, maximum urinary flow rate.

Table 5. Interphenotype comparison of ΔIPSS and ΔQmax in patients with total prostate volume <80 mL

Outcome	Glandular	Mixed	Stromal	*P	**P	***P	****P
ΔQmax 3 m	6.50 ± 3.03	5.58 ± 2.92	3.74 ± 1.65	0.064	0.359	0.006	0.092
ΔQmax 6 m	10.11 ± 2.13	8.17 ± 2.74	7.29 ± 2.66	0.017	0.025	0.007	0.429
ΔQmax 12 m	9.95 ± 1.93	8.36 ± 2.55	7.67 ± 2.56	0.041	0.043	0.017	0.513
ΔQmax 24 m	9.02 ± 2.30	7.15 ± 2.92	6.14 ± 2.74	0.025	0.041	0.009	0.392
ΔIPSS 3 m	8.00 ± 2.60	6.37 ± 2.22	5.56 ± 3.84	0.072	0.050	0.065	0.482
ΔIPSS 6 m	14.12 ± 3.39	9.47 ± 2.44	8.89 ± 3.66	< 0.001	<0.001	0.001	0.618
ΔIPSS 12 m	14.06 ± 3.44	12.63 ± 3.70	10.11 ± 4.34	0.047	0.240	0.018	0.123
ΔIPSS 24 m	13.82 ± 3.84	10.53 ± 3.44	9.89 ± 3.37	0.010	0.010	0.016	0.649

*P, overall three-phenotype comparison; **P, glandular vs. mixed; ***P, glandular vs. stromal; ****P, mixed vs. stromal. IPSS, International Prostate Symptom Score; ΔQmax, maximum urinary flow rate.

Table 6. Interphenotype comparison of ΔIPSS and ΔQmax in patients with total prostate volume ≥ 80 mL

Outcome	Glandular	Mixed	Stromal	*P	**P	***P	****P
ΔQmax 3 m	6.70 ± 2.81	6.11 ± 2.61	5.01 ± 1.66	0.025	0.342	0.004	0.033
ΔQmax 6 m	10.61 ± 2.42	8.39 ±2.23	7.39 ± 1.65	<0.001	<0.001	<0.001	0.043
ΔQmax 12 m	9.68 ± 2.48	8.71 ± 2.08	7.74 ± 1.60	0.002	0.064	<0.001	0.031
ΔQmax 24 m	8.67 ± 2.54	7.60 ± 2.38	6.39 ± 1.72	<0.001	0.058	0.015	0.036
ΔIPSS 3 m	7.44 ± 3.13	6.74 ± 2.56	6.28 ± 2.36	0.218	0.276	0.101	0.443
ΔIPSS 6 m	14.11 ± 5.00	10.24 ±3.03	9.59 ± 2.24	<0.001	<0.001	<0.001	0.328
ΔIPSS 12 m	13.14 ± 3.44	12.24 ± 4.03	11.38 ± 3.60	0.170	0.296	0.049	0.360
ΔIPSS 24 m	12.67 ± 4.48	11.10 ± 3.66	9.55 ± 2.98	0.006	0.092	<0.001	0.064

*P, overall three-phenotype comparison; **P, glandular vs. mixed; ***P, glandular vs. stromal; ****P, mixed vs. stromal. IPSS, International Prostate Symptom Score; ΔQmax, maximum urinary flow rate.

Discussion

This study demonstrates that MRI-defined prostatic morphological phenotypes are strongly associated with differential symptomatic and functional outcomes following PAE. Across the entire cohort, all morphology groups experienced significant improvements in ΔIPSS and ΔQmax, but the magnitude and timing of response varied markedly by phenotype. The glandular-dominant phenotype exhibited the most pronounced and earliest improvement, with maximal gains in both ΔIPSS and ΔQmax achieved by 6 months and sustained through 24 months. By contrast, stromal-dominant prostates exhibited smaller and delayed benefits, typically peaking at around 12 months, whereas mixed morphologies demonstrated intermediate responses. Multivariable regression confirmed that glandular-dominant morphology remained an independent predictor of greater ΔQmax after adjusting for age, baseline prostate volume, and baseline symptom severity, and interaction analysis revealed that this effect was especially pronounced among patients with severe baseline symptoms (IPSS ≥ 20). These findings collectively indicate that preprocedural MRI-based phenotyping can stratify functional recovery trajectories following PAE, providing non-invasive insight into the biological variability of the embolization response.

BPH demonstrates marked histological heterogeneity, with varying proportions of glandular epithelial and stromal components. This compositional variability correlates with differences in LUTS severity and therapeutic efficacy, including outcomes after PAE.[16,23] Considerable interpatient variation in post-PAE symptom relief and urinary flow was identified, which may be attributable to differences in nodular histologic architecture, underscoring the need to investigate morphology-specific treatment effects.

Prior studies have highlighted the prognostic relevance of AdBPH morphology. Patients with AdBPH have demonstrated significantly greater reductions in symptom scores and prostate volume following PAE than those exhibiting non-AdBPH phenotypes.[24] However, most existing studies have relied on binary classification frameworks (AdBPH vs. non-AdBPH) that overlook the histologic heterogeneity of hyperplastic nodules.

To address this limitation, we introduced a three-type MRI-based morphological classification—glandular, stromal, and mixed types—based on nodular composition and signal characteristics on T2-weighted sequences. Radiologic–pathologic correlation studies provide validation for this model. Notably, Dai et al.[16] demonstrated that stromal hyperplasia presents as low-signal, solid tissue on T2-weighted MRI, whereas glandular hyperplasia appears hyperintense with cystic components, facilitating non-invasive differentiation of tissue composition using MRI.

Histologically, glandular-dominant nodules exhibit a high epithelial-to-stromal ratio and a secretory glandular architecture, a histologic profile that demonstrates minimal variation across different prostate volumes.[25] By contrast, stromal-dominant nodules are characterized by an abundance of fibromuscular and fibroblastic elements, rich in smooth muscle and extracellular matrix, and minimal glandular content. Recent spatial and transcriptomic studies have confirmed this histologic phenotype, demonstrating increased expression of *ACTA2*, *VIM*, and collagen genes within stromal-dominant regions.[26,27]

This histological heterogeneity likely contributes to the variability in therapeutic efficacy observed among different nodule subtypes after PAE. Longitudinal analyses across the 24-month follow-up period revealed that prostates with glandular-dominant morphology exhibited significantly earlier and greater improvements in both the IPSS and Qmax than stromal-dominant or mixed types. Incorporating a tripartite MRI-based morphological classification thus allows a more refined interpretation of tissue-specific responses to embolization.

Descriptive and subgroup analyses revealed that glandular-dominant phenotypes reached peak improvements in ΔIPSS and ΔQmax at 6 months following PAE. By contrast, mixed and stromal-dominant phenotypes exhibited delayed peak responses at approximately 12 months. The slower improvement observed in stromal and mixed morphologies—characterized by a greater proportion of fibrous and smooth muscle elements—is likely attributable to reduced susceptibility to ischemic necrosis and delayed tissue remodeling following ischemic injury. Dense stromal tissue may resist ischemic degeneration and exhibit slower clearance of cellular debris, thereby postponing the onset of glandular atrophy and luminal decompression. Consequently, symptomatic relief and improvements in urinary flow emerge more gradually in these phenotypes than in glandular-dominant tissue, which undergoes more rapid ischemic shrinkage and volumetric regression. Preclinical canine models have demonstrated that prostatic artery occlusion induces acute hemorrhagic necrosis and inflammatory infiltration within 2 weeks, followed by progressive glandular atrophy and interstitial fibrotic remodeling by 6 months post-treatment.[28] Histological studies in human participants further support these findings, showing that ischemic necrosis, squamous metaplasia, and inflammation predominantly affect glandular regions, whereas stromal tissue displays relatively limited histopathologic alterations.[29]

At 24 months, both ΔIPSS and ΔQmax demonstrated a modest decline compared with earlier timepoints, indicating a gradual attenuation of the treatment effect across all morphology phenotypes. Despite this reduction in absolute effect size, interphenotype differences remained significant, with the glandular-dominant group consistently exhibiting the most pronounced and durable improvements in both symptomatic and functional outcomes. These findings reinforce the association between glandular-predominant morphology and greater, more sustained responsiveness to PAE. Although the overall treatment effect diminished slightly over time, clinically meaningful benefits relative to baseline were maintained in most patients. This longitudinal trend aligns with prior studies reporting that maximal symptomatic relief typically occurs within the first postoperative year, followed by mild attenuation while preserving overall therapeutic efficacy.[20]

Given that unadjusted analyses are inherently susceptible to confounding by baseline characteristics—such as age, baseline TPV, and initial IPSS or Qmax—multivariable regression modeling was employed to minimize these effects. These adjusted analyses confirmed that glandular-dominant morphology independently predicted greater symptomatic ΔIPSS and functional ΔQmax improvement, with the strongest effects observed during the first postoperative year. By contrast, the mixed-morphology phenotype showed only partial associations, displaying isolated gains in ΔQmax at certain timepoints but no consistent relationship with ΔIPSS. These findings suggest that mixed-type prostates provide variable and less durable functional benefits than the robust and sustained improvements observed in glandular-dominant cases. The predictive association between glandular morphology and ΔIPSS attenuated at 24 months, implying that long-term symptom relief may be influenced by additional pathophysiologic or behavioral factors beyond intrinsic nodule composition. This observation is consistent with findings from the STREAM trial, which reported that patients with stromal-predominant BPH experienced greater symptomatic improvement over prolonged follow-up despite the early advantages observed in adenomatous-dominant cases.[30]

The choice of 80 mL as the prostate volume threshold was driven by clinical convention rather than statistical optimization. From a surgical perspective, international LUTS/BPH guidelines recommend transurethral procedures (e.g., TURP and transurethral laser vaporization) primarily for prostate volumes in the range of 30–80 mL, whereas glands exceeding 80 mL generally require enucleation-based techniques or open/robotic simple prostatectomy, thereby defining ≥ 80 mL as "large-volume" BPH in routine practice. This surgical distinction has been increasingly included in the endovascular literature. Several prospective PAE studies have specifically evaluated cohorts with prostate volumes ≥ 80 mL, reporting meaningful symptom improvement and volume reduction in this population. Thus, using 80 mL as a stratification threshold allows our findings to be interpreted within both guideline-supported clinical boundaries and the established PAE evidence base. Importantly, this classification does not imply a biological transition at 80 mL but serves as a pragmatic cut-off that reflects current clinical decision-making.[18,31,32]

Subgroup analyses stratified by baseline TPV (< 80 vs. ≥ 80 mL) were directionally consistent with the overall results, confirming a morphology-dependent gradient in treatment efficacy. The most pronounced and consistent differences were observed between glandular- and stromal-dominant phenotypes, with glandular-dominant prostates showing superior functional improvements across follow-up intervals. Differences between glandular and mixed morphologies achieved statistical significance at selected timepoints, reflecting the inherent histologic heterogeneity and variable responsiveness characteristic of mixed-type tissue composition.

Consistent with the multivariable regression analyses, mixed and stromal-dominant phenotypes demonstrated no significant differences in most subgroup comparisons, particularly for ΔIPSS. Among patients with larger prostates (≥ 80 mL), significant intergroup variation in ΔQmax emerged as early as 3 months after PAE and persisted throughout the follow-up period. By contrast, patients with smaller prostates (< 80 mL) exhibited no early intergroup differences. These findings highlight a morphology- and volume-dependent gradient in treatment efficacy, supporting the value of combining imaging-based phenotyping with volumetric assessment for personalized therapeutic planning in BPH.

Interaction analysis revealed that only the coexistence of a baseline IPSS ≥ 20 and glandular-dominant morphology independently predicted greater symptomatic improvement at 24 months. Neither baseline symptom severity nor glandular morphology alone showed a significant association with long-term outcomes. These findings suggest that patients with both severe baseline symptoms and glandular-dominant nodules are most likely to achieve durable clinical benefit after PAE. In agreement with prior studies, individuals presenting with more severe LUTS demonstrated the largest long-term reductions in IPSS following embolization.[33,34]

From a clinical perspective, these results underscore the utility of MRI-based prostate morphology classification as a practical tool for patient stratification. Glandular-dominant phenotypes were associated with the most consistent improvements in both symptom scores and urinary flow, whereas mixed phenotypes showed intermediate responses, and stromal-dominant morphology was linked to the least favorable outcomes. Incorporating MRI-based tissue phenotyping into preprocedural evaluation may therefore enhance individualized treatment planning and improve the prediction of clinical response in the management of BPH.

This study has several limitations. First, the morphological classification of BPH nodules was based on a reader-dependent visual assessment of T2-weighted MRI signal characteristics without histopathological validation, introducing potential interobserver variability. Second, the retrospective and single-center design inherently increases the risk of selection bias and residual confounding despite statistical adjustment using multivariable regression modeling. Third, longitudinal measurements of post-void residual volume and prostate size were inconsistently obtained during follow-up, limiting evaluation of their temporal relationships with clinical outcomes. Fourth, other potentially relevant modifiers of treatment response—such as urodynamic parameters, intravesical prostatic protrusion, and systemic or local inflammatory markers—were not routinely assessed or included in the analysis. These unmeasured factors may contribute to interpatient heterogeneity in treatment outcomes and warrant systematic evaluation in future prospective research. Finally, the post-PAE outcome assessment in this retrospective cohort was limited to symptomatic and functional parameters (ΔIPSS and ΔQmax) without uniform post-contrast MRI to quantify ischemic necrosis. Although quantitative necrosis mapping could further elucidate the mechanistic link between baseline morphology and treatment response, post-emboliza-

tion contrast-enhanced imaging was inconsistently obtained in routine care, precluding robust volumetric analysis without selection bias. Future prospective studies with standardized post-PAE MRI (e.g., contrast-enhanced, perfusion, or quantitative mapping) are warranted to test whether morphology influences the extent and pattern of tissue infarction and mediates clinical benefits.

In conclusion, the present findings demonstrate that the histologic composition inferred from the dominant imaging characteristics of transition zone nodules influences both symptomatic and functional outcomes after PAE. Multiparametric MRI, assessed primarily on T2WI, offers a potential non-invasive method for characterizing prostate tissue composition and guiding treatment selection. Although further validation in prospective, multicenter cohorts is warranted, this imaging-based phenotyping framework may assist in identifying histologic phenotypes most likely to achieve favorable therapeutic responses.

Footnotes

Conflict of interest disclosure

The authors declared no conflicts of interest.

References

1. Knight GM, Talwar A, Salem R, Mouli S. Systematic review and meta-analysis comparing prostatic artery embolization to gold-standard transurethral resection of the prostate for benign prostatic hyperplasia. *Cardiovasc Intervent Radiol*. 2021;44(2):183-193. [Crossref]
2. Alemu MH. Transurethral resection of the prostate (TURP)--in the treatment of benign prostatic hypertrophy (BPH) in Mekelle, Ethiopia. *Ethiop Med J*. 2009;47(1):65-69. [Crossref]
3. Ray AF, Powell J, Speakman MJ, et al. Efficacy and safety of prostate artery embolization for benign prostatic hyperplasia: an observational study and propensity-matched comparison with transurethral resection of the prostate (the UK-ROPE study). *BJU Int*. 2018;122(2):270-282. [Crossref]
4. Carnevale FC, Moreira AM, de Assis AM, et al. Prostatic artery embolization for the treatment of lower urinary tract symptoms due to benign prostatic hyperplasia: 10 years' experience. *Radiology*. 2020;296(2):444-451. [Crossref]
5. Müllhaupt G, Hechelhammer L, Graf N, et al. Prostatic artery embolisation versus transurethral resection of the prostate for benign prostatic obstruction: 5-year outcomes of a randomised, open-label, noninferiority trial. *Eur Urol Focus*. 2024;10(5):788-795. [Crossref]
6. Sun F, Lucas-Cava V, Sánchez-Margallo FM. Clinical predictive factors in prostatic artery embolization for symptomatic benign prostatic hyperplasia: a comprehensive review. *Transl Androl Urol*. 2020;9(4):1754-1768. [Crossref]
7. Turkbey B, Rosenkrantz AB, Haider MA, et al. Prostate Imaging Reporting and Data System version 2.1: 2019 update of Prostate Imaging Reporting and Data System version 2. *Eur Urol*. 2019;76(3):340-351. [Crossref]
8. Gaudiano C, Rustici A, Corcioni B, et al. PI-RADS version 2.1 for the evaluation of transition zone lesions: a practical guide for radiologists. *Br J Radiol*. 2022;95(1131):20210916. [Crossref]
9. Li MJ, Hsu HS, Liang RC, Lin SY. Infrared microspectroscopic detection of epithelial and stromal growth in the human benign prostatic hyperplasia. *Ultrastruct Pathol*. 2002;26(6):365-370. [Crossref]
10. Little MW, Boardman P, Macdonald AC, et al. Adenomatous-dominant benign prostatic hyperplasia (AdBPH) as a predictor for clinical success following prostate artery embolization: an age-matched case-control study. *Cardiovasc Intervent Radiol*. 2017;40(5):682-689. [Crossref]
11. Boschheidgen M, Al-Monajjed R, Minko P, et al. Influence of benign prostatic hyperplasia patterns detected with MRI on the clinical outcome after prostatic artery embolization. *CVIR Endovasc*. 2023;6(1):9. [Crossref]
12. Chatterjee A, Gallan AJ, He D, et al. Revisiting quantitative multi-parametric MRI of benign prostatic hyperplasia and its differentiation from transition zone cancer. *Abdom Radiol (NY)*. 2019;44(6):2233-2243. [Crossref]
13. Zumstein V, Betschart P, Vetterlein MW, et al. Prostatic artery embolization versus standard surgical treatment for lower urinary tract symptoms secondary to benign prostatic hyperplasia: a systematic review and meta-analysis. *Eur Urol Focus*. 2019;5(6):1091-1100. [Crossref]
14. Noworolski SM, Vigneron DB, Chen AP, Kurhanewicz J. Dynamic contrast-enhanced MRI and MR diffusion imaging to distinguish between glandular and stromal prostatic tissues. *Magn Reson Imaging*. 2008;26(8):1071-1080. [Crossref]
15. Oto A, Kayhan A, Jiang Y, et al. Prostate cancer: differentiation of central gland cancer from benign prostatic hyperplasia by using diffusion-weighted and dynamic contrast-enhanced MR imaging. *Radiology*. 2010;257(3):715-723. [Crossref]
16. Dai JC, Morgan TN, Goueli R, et al. MRI features associated with histology of benign prostatic hyperplasia nodules: generation of a predictive model. *J Endourol*. 2022;36(3):381-386. [Crossref]
17. Li M, Gao Q, Yu T. Kappa statistic considerations in evaluating inter-rater reliability between two raters: which, when and context matters. *BMC Cancer*. 2023;23(1):799. [Crossref]
18. Bhatia S, Sinha VK, Harward S, Gomez C, Kava BR, Parekh DJ. Prostate artery embolization in patients with prostate volumes of 80 ml or more: a single-institution retrospective experience of 93 patients. *J Vasc Interv Radiol*. 2018;29(10):1392-1398. [Crossref]
19. Veyg D, Mohanka R, Rumball IP, et al. Comparison of 24-month clinical outcomes after prostatic artery embolization in prostate glands larger versus smaller than 80 mL: a systematic review. *J Vasc Interv Radiol*. 2023;34(4):578-584.e1. [Crossref]
20. Neymark AI, Karpenko AA, Neymark BA, et al. Superselective prostatic artery embolization in the treatment of large benign prostatic hyperplasia. *Urologia*. 2021;88(4):374-381. [Crossref]
21. von Elm E, Altman DG, Egger M, et al. The Strengthening the Reporting of Observational Studies in Epidemiology (STROBE) statement: guidelines for reporting observational studies. *J Clin Epidemiol*. 2008;61(4):344-349. [Crossref]
22. Yassin A, Kelly D, Nettleship J, et al. Testosterone treatment and change of categories of the International prostate symptom score (IPSS) in hypogonadal patients: 12 years prospective controlled registry study. *Aging Male*. 2023;26(1):2220567. [Crossref]
23. Diaz TA, Benson B, Clinkenbeard A, Long JR, Kawashima A, Yano M. MRI evaluation of patients before and after interventions for benign prostatic hyperplasia: an update. *AJR Am J Roentgenol*. 2022;218(1):88-99. [Crossref]
24. Strand DW, Costa DN, Francis F, Ricke WA, Roehrborn CG. Targeting phenotypic heterogeneity in benign prostatic hyperplasia. *Differentiation*. 2017;96:49-61. [Crossref]
25. Bauman TM, Nicholson TM, Abler LL, et al. Characterization of fibrillar collagens and extracellular matrix of glandular benign prostatic hyperplasia nodules. PLoS One. 2014;9(10):e109102. [Crossref]
26. Cao Y, Zhang H, Tu GL, et al. The symptoms of benign prostatic hyperplasia patients with stromal-dominated hyperplasia nodules may be associated with prostate fibrosis. Int J Gen Med. 2023;16:1181-1191. [Crossref]
27. Pollack AS, Kunder CA, Brazer N, et al. Spatial transcriptomics identifies candidate stromal drivers of benign prostatic hyperplasia. JCI Insight. 2024;9(2):e176479. [Crossref]
28. Lucas-Cava V, Sanchez-Margallo FM, Moreno-Lobato B, et al. Prostatic artery occlusion: initial findings on pathophysiological response in a canine prostate model. Transl Androl Urol. 2022;11(12):1655-1666. [Crossref]
29. Camara-Lopes G, Mattedi R, Antunes AA, et al. The histology of prostate tissue following

prostatic artery embolization for the treatment of benign prostatic hyperplasia. Int Braz J Urol. 2013;39(2):222-227. [Crossref]

30. Tapping CR, Little MW, Macdonald A, et al. The STREAM Trial (Prostatic Artery Embolization for the Treatment of Benign Prostatic Hyperplasia) 24-month clinical and radiological outcomes. Cardiovasc Intervent Radiol. 2021;44(3):436-442. [Crossref]
31. Wang M, Guo L, Duan F, et al. Prostatic arterial embolization for the treatment of lower urinary tract symptoms caused by benign prostatic hyperplasia: a comparative study of medium- and large-volume prostates. BJU Int. 2016;117(1):155-164. [Crossref]
32. Gravas S, Gacci M, Gratzke C, et al. Summary paper on the 2023 European Association of Urology Guidelines on the management of non-neurogenic male lower urinary tract symptoms. Eur Urol. 2023;84(2):207-222. [Crossref]
33. Thulasidasan N, Kok HK, Elhage O, Clovis S, Popert R, Sabharwal T. Prostate artery embolisation: an all-comers, single-operator experience in 159 patients with lower urinary tract symptoms, urinary retention, or haematuria with medium-term follow-up. Clin Radiol. 2019;74(7):569.e1-569.e8. [Crossref]
34. Moreira AM, de Assis AM, Carnevale FC, Oliveira DS, Antunes AA. Improvements in irritative versus obstructive symptoms of the international prostate symptom score after prostatic artery embolization in 174 patients, in a single center. Cardiovasc Intervent Radiol. 2020;43(4):613-619. [Crossref]